ChemistryOPEN

# Supporting Information



# Understanding the Molecular Structure of the Sialic Acid–Phenylboronic Acid Complex by using a Combined NMR Spectroscopy and DFT Study: Toward Sialic Acid Detection at Cell Membranes

Shoichi Nishitani, Yuki Maekawa, and Toshiya Sakata*[a]

open_201800071_sm_miscellaneous_information.pdf

## S1. Introduction (Supporting Information)

Nuclear magnetic resonance (NMR) spectroscopy is a well-known powerful tool for molecular structural analysis. In fact, $^{1}H$ and $^{13}C$ NMR has been used to determine the structure of sialic acid (SA) in aqueous solutions[1,2] and monosaccharide/phenylboronic acid (PBA) complex structures.[3,4] In particular, $^{11}B$ NMR is also a useful tool for diol/PBA complexation as the complexation reaction is relatively slow compared with the NMR time-scale; thus, the diol/PBA complex peak and PBA free peak are observed as two distinct peaks.[5,6] From these results, the occurrence of the complexation can be clarified, and the conditional formation constant can be determined in this study. In past studies, only NMR was used to determine the SA/PBA major complex structure. However, it is difficult, if not impossible, to fully elucidate the structures and conformations of the sugar/PBA complex structure only from NMR analysis because of the complexity of the spectral data[7] Therefore, we also performed density functional theory (DFT) simulations to support our experimental results and to fully determine the stable conformation. In the DFT simulations, the electronic structures of molecules are calculated, information about energies, frequencies, magnetic properties, and so forth. DFT simulation is a powerful tool widely used in various fields because the simulation results are comparatively accurate considering the short calculation time. In this study, DFT simulations were performed for two reasons: to calculate $^{11}B$ and $^{13}C$ NMR spectra to support the complex experimental results, and to calculate the static atomistic structure of the SA/PBA complex to compare the stability of each complex structure as well as to visualize the stable conformation.

## S2. $^{11}$B NMR spectra and conditional formation constant

Conditional formation constant (*K*) is a useful index to tell whether the complexation between PBA and the ligand occurs or not.[8] The conditional formation constant for SA/PBA complex is determined by the following equation at a certain pH.[9]

$$K = \frac{[complex]}{[PBA]_{free}[SA]_{free}} \tag{1}$$

In the equation, [complex] shows the total concentration of the complex structures of all forms, $[PBA]_{free}$ shows the total concentration of free $B(OH)_2$ and $B(OH)_3^-$, and $[SA]_{free}$ shows the total concentration of free SA of all forms, all at the equilibrium. If we let $[PBA]_0$ and $[SA]_0$ as initial concentration of PBA and SA, respectively, and *r* equals to the ratio of $[PBA]_{free}$ and [complex], we can relate them in the following equations.

$$r = \frac{[PBA]_{free}}{[complex]} \tag{2}$$

$$[PBA]_0 = [PBA]_{free} + [PBA]_{complex} \tag{3}$$

$$[SA]_0 = [SA]_{free} + [SA]_{complex} \tag{4}$$

$$[complex] = [PBA]_{complex} = [SA]_{complex} \tag{5}$$

Then, *K* can be written in the following relationship:

$$K = \frac{1+r}{r\{(1+r)[SA]_0 - [PBA]_0\}} \tag{6}$$

The peak integral of the NMR spectra is proportional to the concentration of the

corresponding molecules. As 2 peaks in $^{11}B$ NMR correspond to the free PBA and SA/PBA complex, the value of *r* can be estimated from the ratio of the peak integrals. Then, *K* can be further determined. The values of *K* for each condition was calculated based on the equations, and listed on Table S1 together with the experimental results.

**Table S1** Profiles of the $^{11}B$ NMR chemical shifts and the estimated values of *K*

| | **Free peak (ppm)** | **Complex peak (ppm)** | **K ($M^{-1}$)** |
|---|---|---|---|
| **SA in organic solvent** | 28.3 | 9.1 | 26.7 |
| **SA in aqueous solvent** | 28.0 | 8.3 | 36.1 |
| **mSA** | 28.3 | N/A | N/A |

## S3. Detailed results of $^{13}C$ NMR spectra

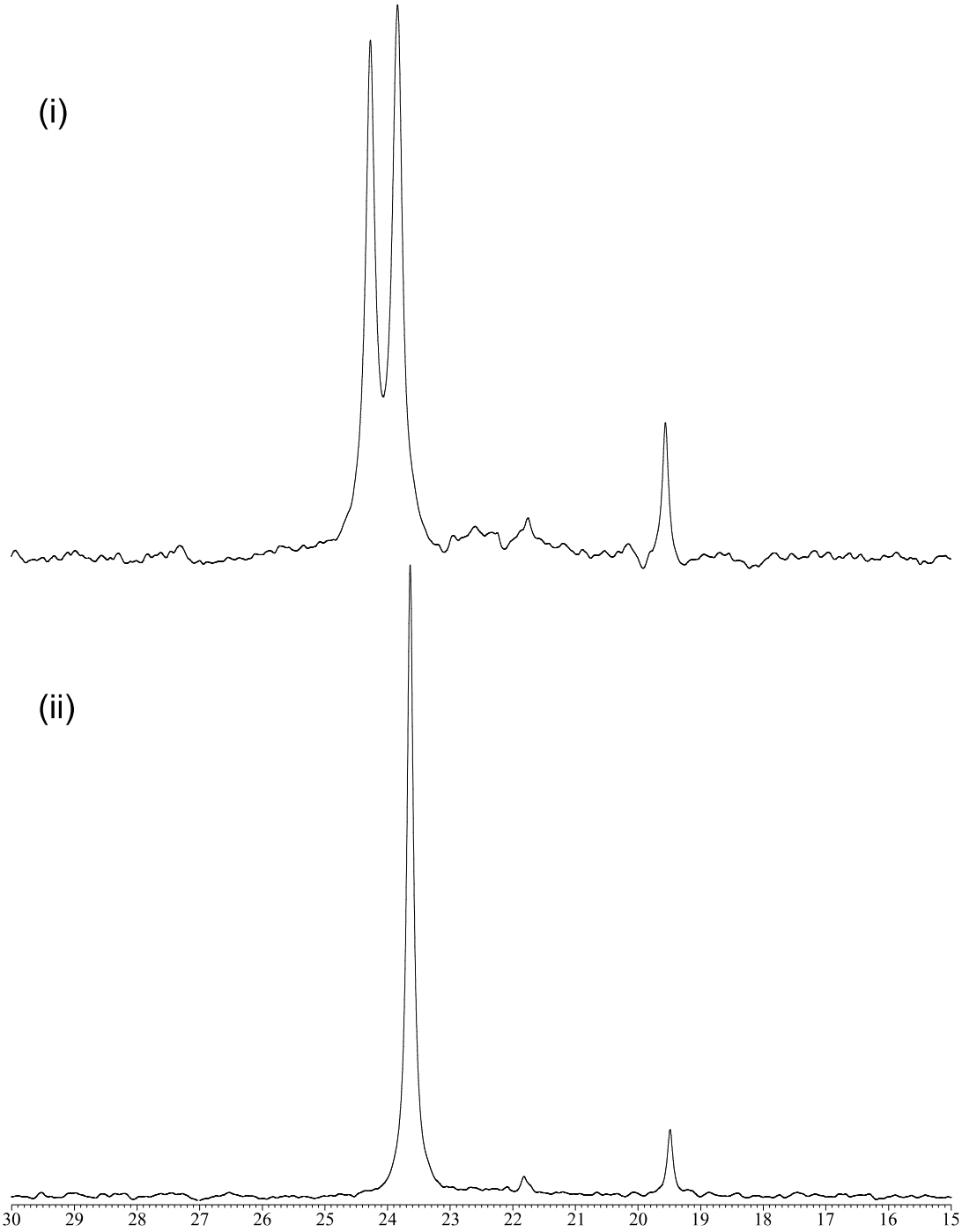


**Fig. S1 (a)** $C_{me}$ peaks of $^{13}C$ NMR spectra of (i) 1M SA/VPBA in DMSO and (ii) 1M SA

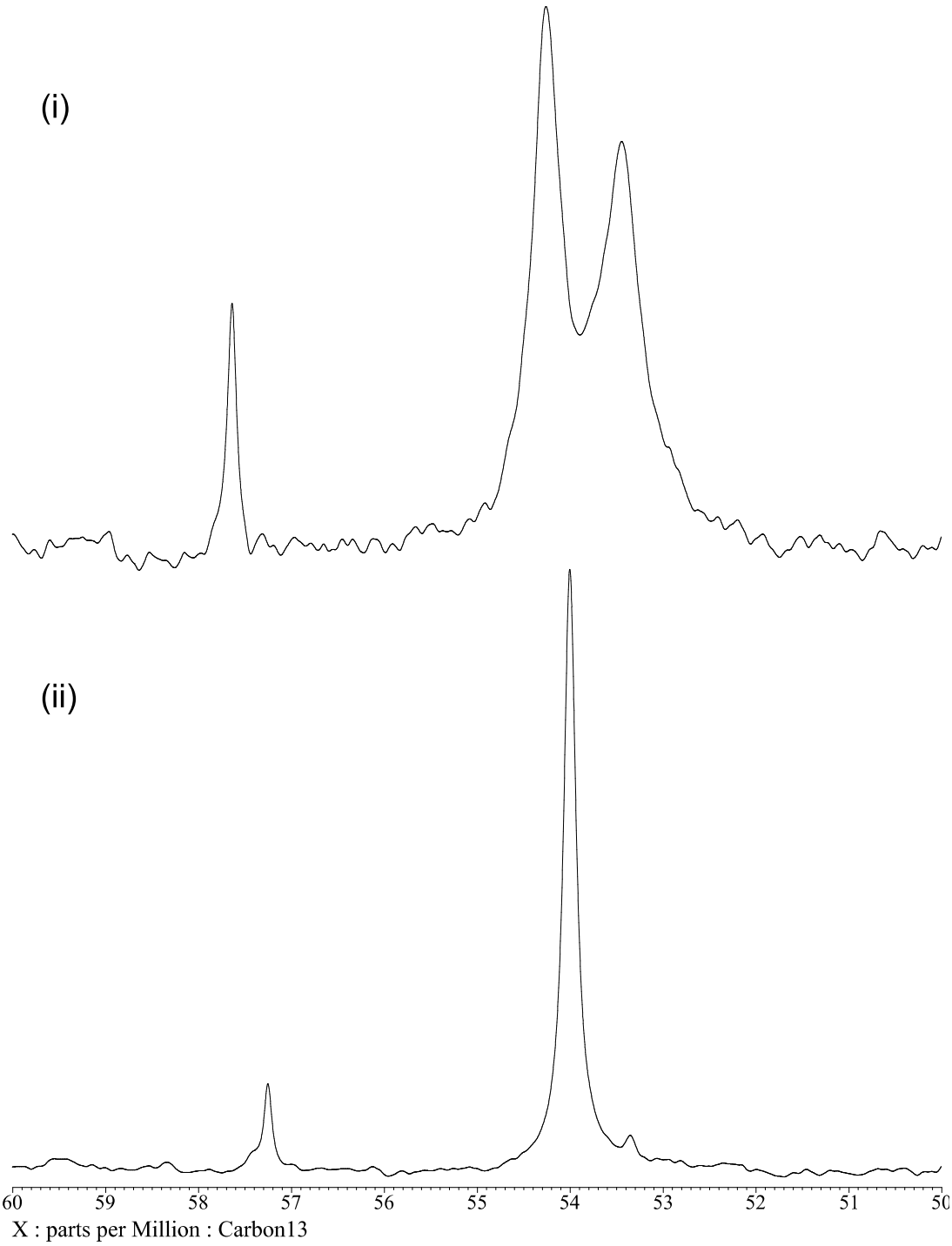


**Fig. S1 (b)** $C_5$ peaks of $^{13}C$ NMR spectra of (i) 1M SA/VPBA in DMSO and (ii) 1M SA

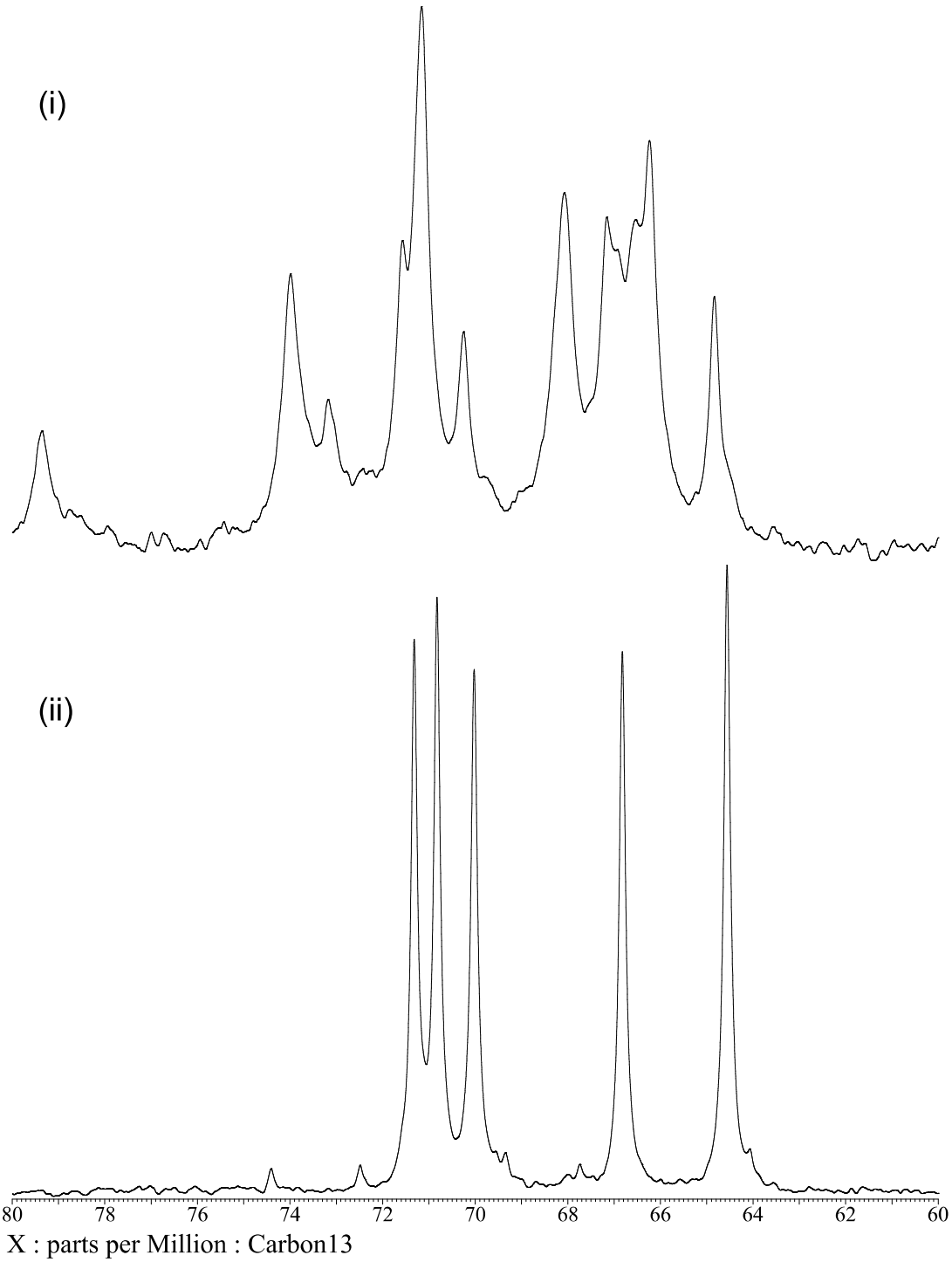


**Fig. S1 (c)** Peaks of hydroxyl carbons ($C_4$, $C_6$, $C_7$, $C_8$, and $C_9$) of $^{13}C$ NMR spectra of (i) 1M SA/VPBA in DMSO and (ii) 1M SA

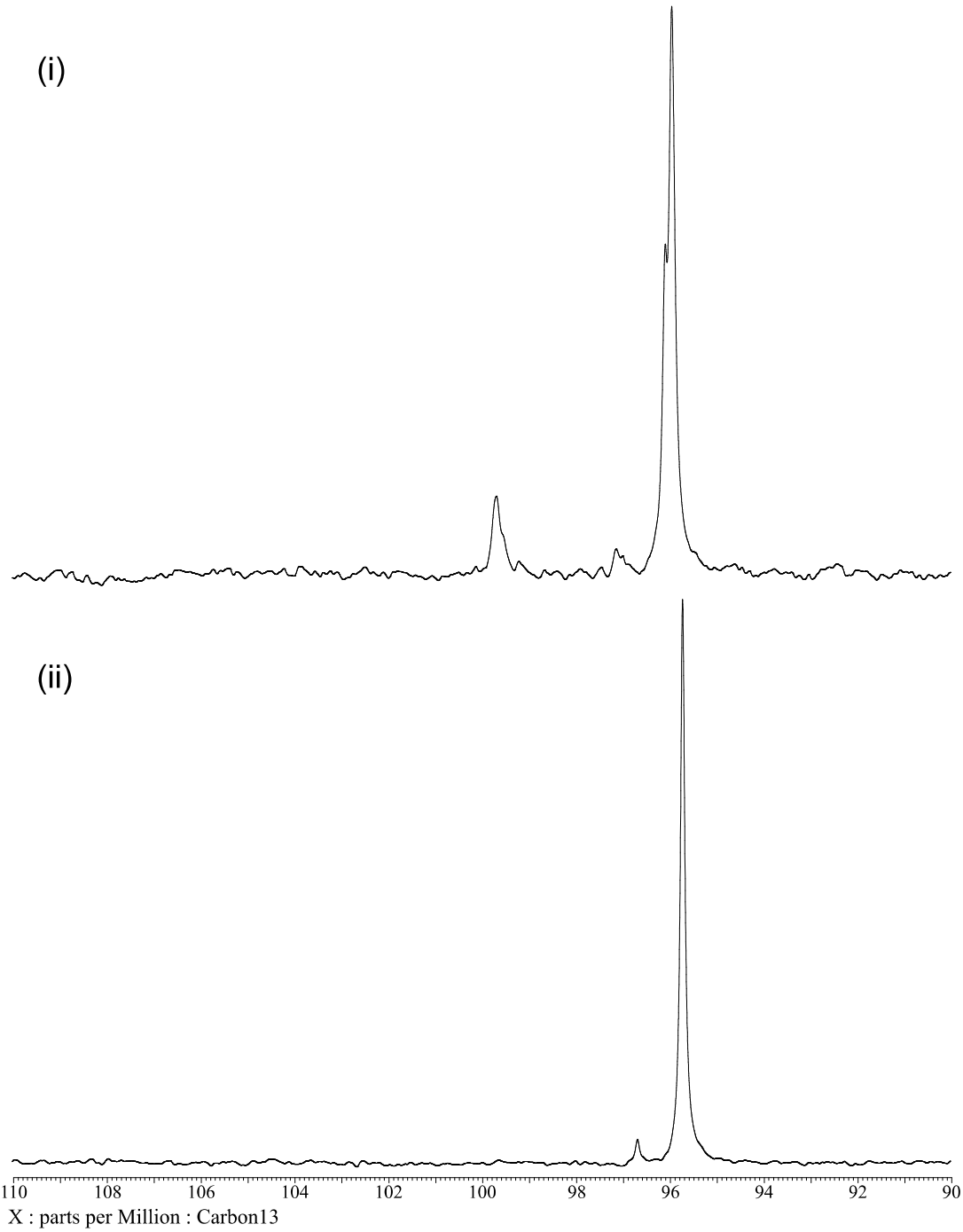


**Fig. S1 (d)** $C_2$ peaks of $^{13}C$ NMR spectra of (i) 1M SA/VPBA in DMSO and (ii) 1M SA

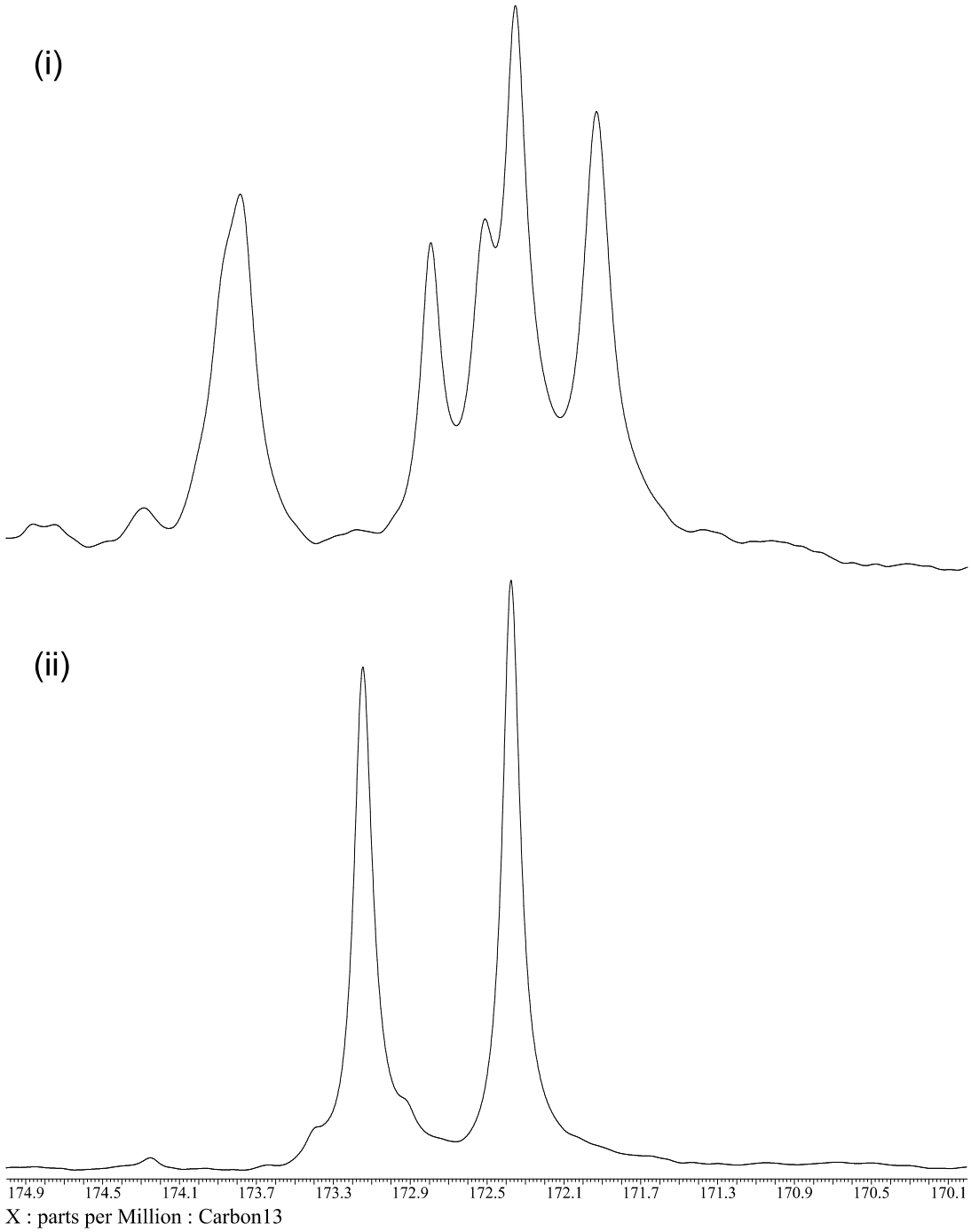


**Fig. S1 (e)** Peaks of carboxyl carbons ($C_1$, and $C_{Ac}$) of $^{13}C$ NMR spectra of(i) 1M SA/VPBA in DMSO and (ii) 1M SA

## S4. Detailed peak profile of $^{13}C$ NMR chemical shifts, and the corresponding chemical shifts calculated by DFT

**Table S2 (a)** Profile of $^{13}C$ NMR chemical shifts of 1 M SA in DMSO

| Carbon | Chemical shift (ppm) |
|---|---|
| αCMe | 19.5 |
| βCMe | 23.6 |
| αC5 | 57.3 |
| βC5 | 54.0 |
| αC9 | 64.0 |
| βC9 | 64.6 |
| αC4 | 67.7 |
| βC4 | 66.8 |
| αC8 | 69.4 |
| βC8 | 70.0 |
| αC6 | 70.8 |
| βC6 | 72.5 |
| αC7 | 74.4 |
| βC7 | 71.3 |
| αC2 | 96.7 |
| βC2 | 95.7 |
| βCAc | 172 |
| βC1 | 173 |

**Table S2 (b)** Profile of $^{13}C$ NMR chemical shifts of 1 M SA and 1 M PBA in DMSO

| Carbon | | Chemical shift (ppm) |
|---|---|---|
| $C_{Me}$ | Free α | 19.6 |
| | Free β | 23.8 |
| | Complex β | 24.3 |
| $C_5$ | Free α | 57.6 |
| | Free β | 54.2 |
| | Complex β | 53.5 |
| $C_4$, $C_6$, $C_7$, $C_8$, $C_9$ | | 64.8 |
| | | 66.2 |
| | | 66.6 |
| | | 67.0 |
| | | 67.2 |
| | | 68.1 |
| | | 70.3 |
| | | 71.2 |
| | | 71.6 |
| | | 73.2 |
| | | 74 |
| | | 79.4 |
| $C_2$ | Free α | 96.1 |
| | Free β | 95.9 |
| | Complex β | 99.7 |
| $C_1$, $CA_c$ | | 171.9 |
| | | 172.3 |
| | | 172.5 |
| | | 172.8 |
| | | 173.8 |

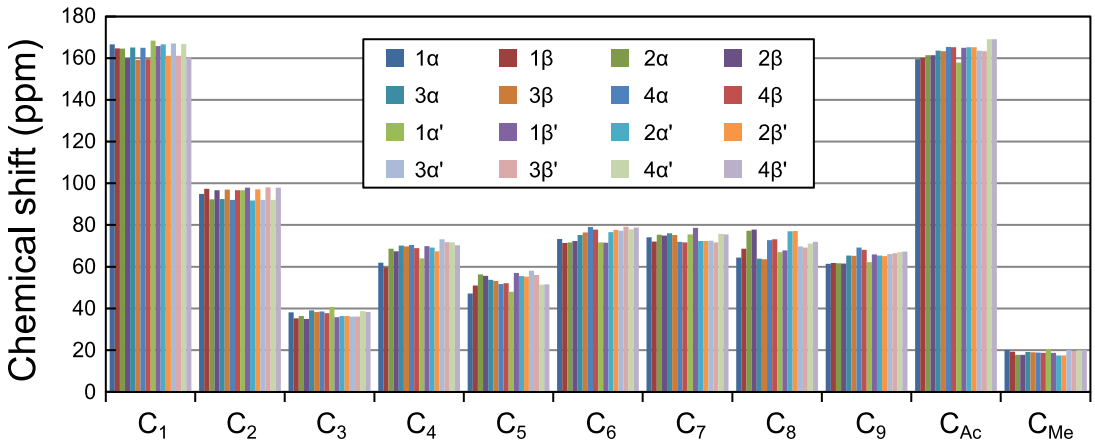


**Fig. S2** $^{13}C$ NMR chemical shifts calculated by DFT. The abbreviation on the caption: 1α, 1β, 2α, 2β, 3α, 3β, 4α, 4β, 1α', 1β', 2α', 2β', 3α', 3β', 4α', 4β' stands for: $\alpha C_1C_2/B(OH)_2$, $\beta C_1C_2/B(OH)_2$, $\alpha C_7C_8/B(OH)_2$, $\beta C_7C_8/B(OH)_2$, $\alpha C_7C_9/B(OH)_2$, $\beta C_7C_9/B(OH)_2$, $\alpha C_8C_9/B(OH)_2$, $\beta C_8C_9/B(OH)_2$, $\alpha C_1C_2/B(OH)_3^-$, $\beta C_1C_2/B(OH)_3^-$, $\alpha C_7C_8/B(OH)_3^-$, $\beta C_7C_8/B(OH)_3^-$, $\alpha C_7C_9/B(OH)_3^-$, $\beta C_7C_9/B(OH)_3^-$, $\alpha C_8C_9/B(OH)_3^-$, and $\beta C_7C_9/B(OH)_3^-$, respectively.

## S5. Relative stability of α-$C_1C_2$/$B(OH)_3^-$ and β-$C_1C_2$/$B(OH)_3^-$

As shown in **Fig. S3**, conformational structure of α-SA, β-SA, α-$C_1C_2$/$B(OH)_3^-$, and β-$C_1C_2$/$B(OH)_3^-$ were optimized using DFT calculation. From the calculation, β-SA turned out to be more stable compared with α-SA by 3.2 kcal/mol. For α-SA, carboxyl group lied on axial conformation, as shown in **Fig. S3(a)**. This caused both steric hindrance and the repulsive interactions between the oxygen atom (=O oxygen) of carboxyl group and the oxygen atoms in the SA ring; thus, the configuration of oxygen atoms resulted in the relative instability of the structure. This was not the case for β-SA (**Fig. S3(b)**) where carboxyl group lied on equatorial conformation; that is, there was no interaction between the corresponding oxygen atoms, so the conformation was energetically stable compared with α-SA. After the complexation, the relative energy difference was calculated to be 2.9 kcal/mol (**Table 2**). This value corresponds to the

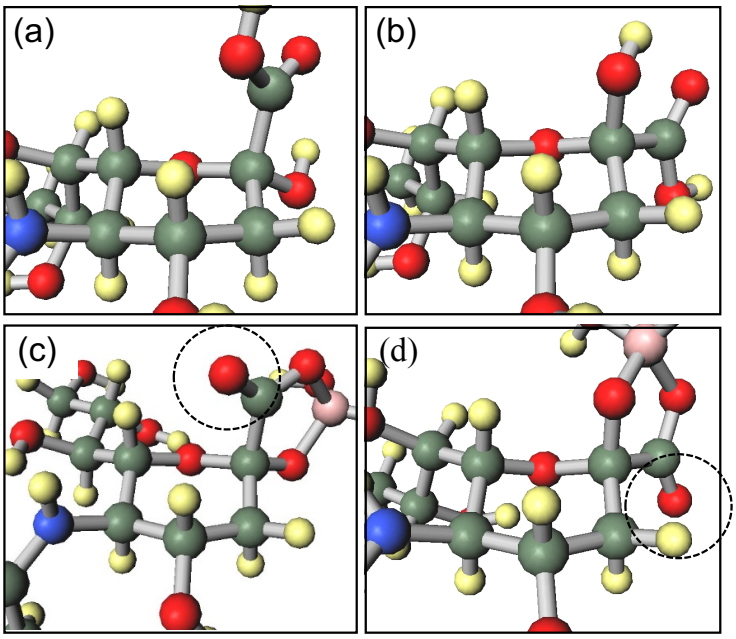


**Fig. S3** Optimized conformational structures of (a) α-SA, (b) β-SA, (c) α-$C_1C_2$/$B(OH)_3^-$, and (d) β-$C_1C_2$/$B(OH)_3^-$ derived from DFT calculations. =O oxygen in carboxyl group of SA is highlighted in each circle.

energy difference between α-SA and β-SA. Even if the SA makes a complex with VPBA, the energetically unfavorableness of α-SA does not eliminate. Thus, the most likely stable conformation of β-$C_1C_2$/$B(OH)_3^-$ was obtained by DFT simulation, as shown in **Figs. S3(d) and 6**.

## References


1. H. Friebolin, P. Kunzelmann, M. Supp, R. Brossmer, G. Keilich and D. Ziegler, *Tetrahedron Lett.*, **1981**, *22*, 1383–1386.
2. H. Schmidt and H. Friebolin, *J. Carbohydr. Chem.*, **1983**, *2*, 405–413.
3. J. C. Norrild, *J. Chem. Soc. Perkin Trans.*, **2001**, *2*, 719–726.
4. M. Bielecki, H. Eggert and J. C. Norrild, *J. Chem. Soc. Perkin Trans.*, **1999**, *2*, 449–456.
5. R. D. Pizer, P. J. Ricatto and C. A. Tihal, *Polyhedron*, **1993**, *12*, 2137–2142.
6. X. Yang, M. C. Lee, F. Sartain, X. Pan and C. R. Lowe, *Chem. - A Eur. J.*, **2006**, *12*, 8491–8497.
7. J. C. Norrild and H. Eggert, *J. Am. Chem. Soc.*, **1995**, *117*, 1479–1484.
8. Y. Furikado, T. Nagahata, T. Okamoto, T. Sugaya, S. Iwatsuki, M. Inamo, H. D. Takagi, A. Odani and K. Ishihara, *Chem. - A Eur. J.*, **2014**, *20*, 13194–13202.
9. H. Otsuka, E. Uchimura, H. Koshino, T. Okano and K. Kataoka, *J. Am. Chem. Soc.*, **2003**, *125*, 3493–3502.
10. W. S. Johnson, V. J. Bauer, J. L. Margrave, M. A. Frisch, L. H. Dreger and W. N. Hubbard, *J. Am. Chem. Soc.*, **1961**, *83*, 606–614.
11. M. Squillacote, R. S. Sheridan, O. L. Chapman and F. A. L. Anet, *J. Am. Chem. Soc.*, **1975**, *97*, 3244–3246.
12. T. W. G. Solomons, J. E. Fernandez, C. B. Fryhle, S. A. Snyder and T. W. G. Solomons, *Organic chemistry. [1], [Hauptbd.]*, Wiley, **2014**.